Title

Nucleocapsid and glycoprotein organization in an enveloped virus

Journal

Cell, 80(4)

ISSN

0092-8674

Authors

Cheng, RH
Kuhn, RJ
Olson, NH
et al.

Publication Date

1995-02-01

DOI

10.1016/0092-8674(95)90516-2

Peer reviewed

Cell, Vol. 80, 621–630, February 24, 1995, Copyright © 1995 by Cell Press

Nucleocapsid and Glycoprotein Organization in an Enveloped Virus

R. Holland Cheng, Richard J. Kuhn, Norman H. Olson, Michael G. Rossmann, Hok-Kin Choi, Thomas J. Smith, and Timothy S. Baker
Department of Biological Sciences
Purdue University
West Lafayette, Indiana 47907

Summary

Alphaviruses are a group of icosahedral, positive-strand RNA, enveloped viruses. The membrane bilayer, which surrounds the ~400 Å diameter nucleocapsid, is penetrated by 80 spikes arranged in a T = 4 lattice. Each spike is a trimer of heterodimers consisting of glycoproteins E1 and E2. Cryoelectron microscopy and image reconstruction of Ross River virus showed that the T = 4 quaternary structure of the nucleocapsid consists of pentamer and hexamer clusters of the capsid protein, but not dimers, as have been observed in several crystallographic studies. The E1-E2 heterodimers form one-to-one associations with the nucleocapsid monomers across the lipid bilayer. Knowledge of the atomic structure of the capsid protein and our reconstruction allows us to identify capsid-protein residues that interact with the RNA, the glycoproteins, and adjacent capsid-proteins.

Introduction

Alphaviruses are a closely related group of positive-strand RNA viruses. These icosahedral viruses have been extensively studied because they represent a model for the simple, enveloped viruses. Ross River virus (RR), one of the 27 members of the alphavirus group, was originally isolated from a pool of Aedes vigilax mosquitoes in 1963 and was also later isolated from infected humans (Doherty et al., 1963). RR has an extremely wide host range, yet it produces clinical symptoms only in humans and mice. It causes epidemic polyarthritis in humans and is endemic to Australia (Kay and Aaskov, 1989). This disease, the symptoms of which include fever, rash, and arthritis in the peripheral joints, has also been reported in the Fiji Islands and American Somoa. Massive outbreaks of the disease occurred in 1979 and 1980 in these islands (Marshall and Miles, 1984). The virus is transmitted by mosquitoes, and the primary reservoir appears to be marsupials and other small mammals.

The sequence of the entire RR genome (11,851 nucleotides, excluding the encoded poly(A) tract) of the prototype T48 strain is known (Dalgarno et al., 1983; Faragher et al., 1988). This strain shares extensive amino acid homology with the closely related Semliki Forest virus (SF) in both structural and nonstructural proteins (73% and 78% amino acid identity, respectively) and, to a lesser extent, with Sindbis virus (SIN) (structural proteins show 48% and nonstructural proteins 64% amino acid identity, respectively). A subgenomic mRNA, synthesized from the 3′ one-third of the genome, serves as the template for the 138 kDa polyprotein, which is processed into four major structural proteins: the ~30 kDa nucleocapsid protein, and the envelope glycoproteins (E1 [~52 kDa], E2 [~49 kDa], and E3 [~10 kDa]). The nucleocapsid protein is responsible for packaging the viral genome RNA into an icosahedral protein shell of ~400 Å diameter. E1 and E2 form heterodimers in all alphaviruses, but the small E3 glycoprotein dissociates from some alphaviruses, such as SIN and RR (Mayne et al., 1984; Vrati et al., 1986), whereas it remains associated with SF (Garoff et al., 1974). Heterodimers associate as trimers (Ziemiecki and Garoff, 1978; Rice and Strauss, 1982) and form eighty spike-like projections that extend outward from the viral membrane (Paredes et al., 1993a). The E1 glycoprotein contains a fusion domain that is probably involved in membrane penetration of the virus (Garoff et al., 1980; Rice and Strauss, 1981). Glycoprotein E2 contains the major epitopes to which neutralization antibodies bind and probably also is involved in virus–cellular receptor interactions (Dalrymple et al., 1976; Ubol and Griffin, 1991; Wang et al., 1991). Both glycoproteins extend completely through the lipid bilayer. E2 has an extended cytoplasmic domain that is believed to contact the capsid core (Garoff and Simons, 1974; Lopez et al., 1994).

Structural studies of alphaviruses at atomic resolution have not yet been possible because the best crystals available only diffract X-rays to ~30 Å resolution (Harrison et al., 1992). Nevertheless, cryoelectron microscopy (cryo-EM) studies have established a triangulation number of four for the outer envelope glycoproteins on both SIN (Fuller, 1987) and SF (Vogel et al., 1986). The T = 4 structure implies that a total of 240 E1–E2 heterodimers cluster as 80 trimers, 60 of which are situated on quasi-threefold axes and 20 on icosahedral threefold axes. This glycoprotein organization is consistent with biochemical data that showed there are two distinct chemical environments for the E1–E2 heterodimer (Helenius and Kartenbeck, 1980; Anthony and Brown, 1991; Vénien-Bryan and Fuller, 1994).

The organization of the nucleocapsid core subunits has been reported as either T = 3 (Horzinek and Mussgay, 1969; Fuller, 1987) or T = 4 (Coombs and Brown, 1987a; Paredes et al., 1993a, 1993b). A T = 3 structure would have nonequivalent associations between the inner nucleocapsid proteins and the envelope glycoproteins, whereas a T = 4 structure would permit stoichometric and quasiequivalent interactions between the nucleocapsid proteins and the glycoproteins. Support for the T = 4 model came from X-ray crystallographic studies of the capsid protein. The ordered portion of the structure was too small to form a stable 400 Å diameter shell with only 180 subunits that would constitute a T = 3 particle (Choi et al., 1991). These observations were further supported by direct mass measurements of nucleocapsid particles obtained with

scanning transmission EM (Paredes et al., 1993b). A recent cryo-EM and image reconstruction study of SIN (Paredes et al., 1993a) showed that it has a similar T = 4 organization and is apparently consistent with the dimeric capsid protein structure observed crystallographically.

The X-ray crystallographic investigation of the SIN capsid protein (SCP) showed that the basic, N-terminal domain (residues 1–113) is disordered, but the remaining C-terminal portion (residues 114–264) is highly ordered (Choi et al., 1991; Tong et al., 1992, 1993). The C-terminal domain of the SCP has a chymotrypsin-like structure, which is responsible for the *cis* cleavage of this protein from the translated polyprotein (Simmons and Strauss, 1974; Aliperti and Schlesinger, 1978). At least two different crystal forms of SCP and SF coat protein (H.-K. C., G. Wengler, and M. G. R., unpublished data) and one form of a truncated RR coat protein expressed in E. coli show the same dimeric state (H.-K. C., R. J. K., and M. G. R., unpublished data), suggesting that the dimer might be a functional unit. The basic N-terminal domain in the alphavirus coat protein has a highly variable sequence in comparison with the conserved C-terminal domain. Sequence identity of residues 114–264 of the nucleocapsid among alphaviruses ranges from 59% identity between SIN and Venezuelan equine encephalitis virus to 100% identity between SIN and Ockelbo virus (Tong et al., 1993). The N-terminal domain of the SCP recognizes viral RNA (Geigenmüller-Gnirke et al., 1993; Weiss et al., 1994) and ribosomal RNA (Wengler et al., 1992) and probably is involved in RNA packaging. The SCP also binds the C-terminal, cytoplasmic domain of E2. Thus, this structural protein functions in at least four different ways: as an enzyme, as a protective coat for the viral genome, as an RNA-binding protein, and as a receptor for the cytoplasmic domain of the transmembrane spike structure.

We report a cryo-EM and image reconstruction study of RR at ~25 Å resolution, which reveals new details about the organization of an alphavirus. The nucleocapsid core consists of monomeric subunits organized as 12 pentamers and 30 hexamers. The atomic model of the C-terminal domain of the SCP fits uniquely into the core region of the virus three-dimensional (3D) density map and has a one-to-one association with the envelope glycoproteins. The lipid bilayer membrane, which is sandwiched between the inner nucleocapsid core and the outer envelope glycoproteins, is clearly visible. Each of the 60 spikes on the quasi-threefold axes is tethered through the membrane to three SCP subunits distributed among two hexamers and one pentamer, whereas each of the 20 spikes on the icosahedral threefold axes is tethered to three SCP subunits on threefold-related hexamers.

Results and Discussion

Cryo-EM and Image Reconstruction

Electron micrographs of RR embedded in vitreous ice (Figure 1) provided a set of 68 particle images from which a 3D reconstruction was computed at 25 Å. The correct hand of the structure was determined from experiments in which RR was tilted in the microscope, and resulting images

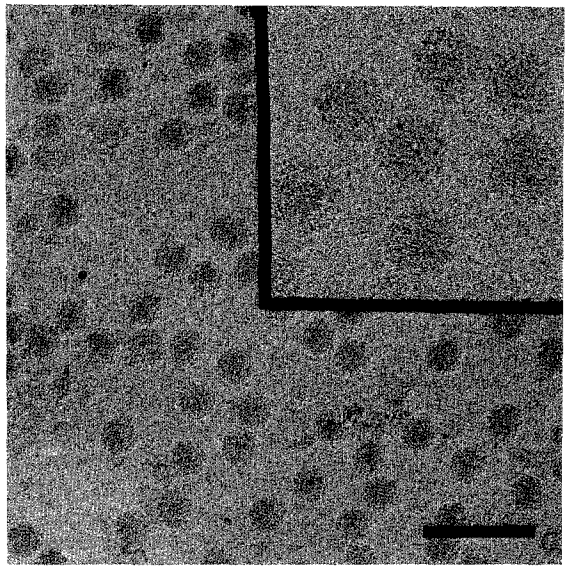

Figure 1. Low Magnification View of Frozen-Hydrated RR Recorded at 1.5 μm Underfocus

The inset shows some RR images that were used in the reconstruction (Figure 2) at <1 μm underfocus. Bar is 2000 Å, and inset is 1000 Å.

were compared by cross-correlation with corresponding projections of left- and right-hand versions of the reconstructions. The improved quality of the RR map, when compared to maps obtained for SIN (Fuller, 1987; Paredes et al., 1993a; N. H. O. and T. J. S., unpublished data) or SF (Vogel et al., 1986; Vénien-Bryan and Fuller, 1994; Kenney et al., 1994), indicates that the icosahedral symmetry of RR is better preserved in the specimen. The difference might be related to RR being propagated in mosquito cells rather than mammalian cells. Alternatively, RR may be more stable during specimen preparation for cryo-EM.

Surface-shaded representations of the RR reconstruction, viewed along twofold and threefold axes, clearly show the threefold nature of the surface spikes and the bilobal nature of each of the spike petals (Figure 2). The surface of the virus is almost exclusively covered by protein, except for prominent holes (50 Å long × 40 Å wide) that expose the surface of the lipid bilayer at the icosahedral twofold axes, 20 Å diameter holes at the fivefold axes, and 15 Å diameter holes at the base of each spike. The organization of the spikes within the T = 4 icosahedral lattice (Figure 2c) is discussed in greater detail below.

Equatorial sections of the reconstruction depict the layered structure of the virion (Figure 3). The density map on its own cannot differentiate between nucleic acid, protein, and lipid components of the virion, but low-angle neutron (Jacrot, 1987) and X-ray (Harrison et al., 1971, 1974; Stubbs et al., 1991) scattering results permit us to ascribe specific features to these components. The scattering data suggested that the glycoproteins are located between radii of 350 Å and 260 Å and that the inner and outer surfaces of the membrane are at 210 Å and between 250 Å (Jacrot, 1987) and 258 Å radius (Harrison et al., 1971), respectively (Figure 3a). Radii between 210 Å and 170 Å

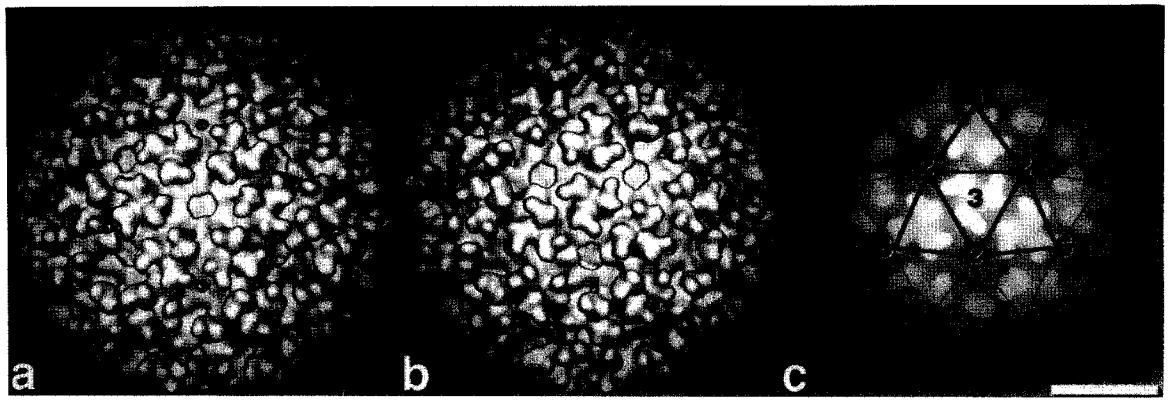

Figure 2. Surface-Shaded and Depth-Cued Representations of the RR Reconstruction

The surface-shaded representations are viewed along a twofold axis (a) and a threefold axis (b). The 3D reconstruction was computed from 68 independent particle images. The depth-cued representation (c), viewed along a threefold axis, is overlaid with a T = 4 lattice to show the relative positions of the glycoprotein spikes with respect to the five-, three-, and twofold symmetry axes (labeled with numbers). Bar is 200 Å. Small holes are also observed on the fivefold axes, and even smaller holes are at the base of each spike.

mainly contain protein, whereas a mixture of protein and RNA occurs at lower radii. The low-angle scattering results permitted us to identify features in the RR reconstruction and ascribe these to the various viral components.

The E1-E2 Glycoprotein Spike

The RR spikes (Figure 4) are similar in size to those previously reported for SF and SIN (Vogel et al., 1986; Fuller, 1987; Paredes et al., 1993a), although they are seen in more detail. They extend 95 Å radially outwards from 255–350 Å. The glycoprotein spike head group has a large, flower-like morphology with bilobal petals the surfaces of which lie within 15 Å of the surfaces of neighboring spikes (see Figure 2; Figures 4a and 4b). The head group has a diameter of ~125 Å. The stem immediately below the head group is ~85 Å in diameter with a roughly triangular cross-section and a 25 Å hole in the center (Figure 4d, cross-section B), demonstrating the trimeric clustering of the spike glycoproteins. At radii less than 290 Å, the glycoproteins skew outwards as separate E1–E2 heterodimers to a diameter of ~125 Å. At a viral radius of 290 Å, all 240 heterodimers are separated, and each one then appears to traverse the membrane to form a specific interaction with a nucleocapsid monomer (see Figure 3). Separation of the individual heterodimers from the stem at the base of the spike opens up lateral holes, about 15 Å in diameter, creating a large cavity that extends 30 Å radially from the membrane to the base of the head group. The current data do not discriminate between the E1 and E2 glycoproteins, although recent studies of alphaviruses

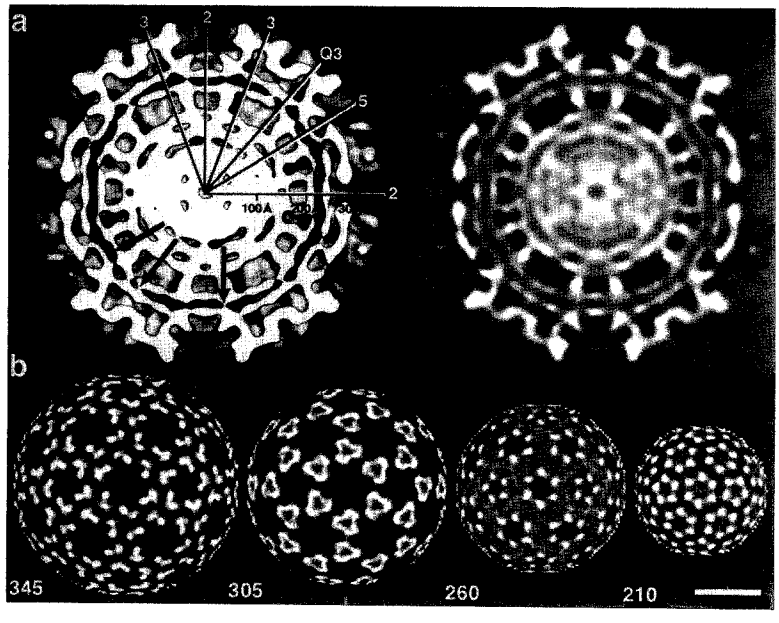

Figure 3. Radial Density Distributions

(a) Equatorial cross-section of the virus reconstruction along a twofold axis, with high density in white and low density (solvent and lipid) in black. The right half is a continuous, grey-level representation of the section, whereas the left half is a surface representation, shaded at a contour level of 0.5 standard deviation above the average. The positions of icosahedral two-, three-, fivefold, and quasi-threefold (Q3) axes are shown along with a scale marker. The closed arrows show regions of membrane pinching suggested to be the location of the transmembrane connections.

(b) Projected density distributions (twofold view) at specific radii of the front half of the RR reconstruction. High to low densities are represented with a white to black grey scale, respectively. Bar is 200 Å. The juxtapositions of the spike glycoproteins (260 Å) and the nucleocapsid (210 Å) at both surfaces of the lipid bilayer are evident in these views.

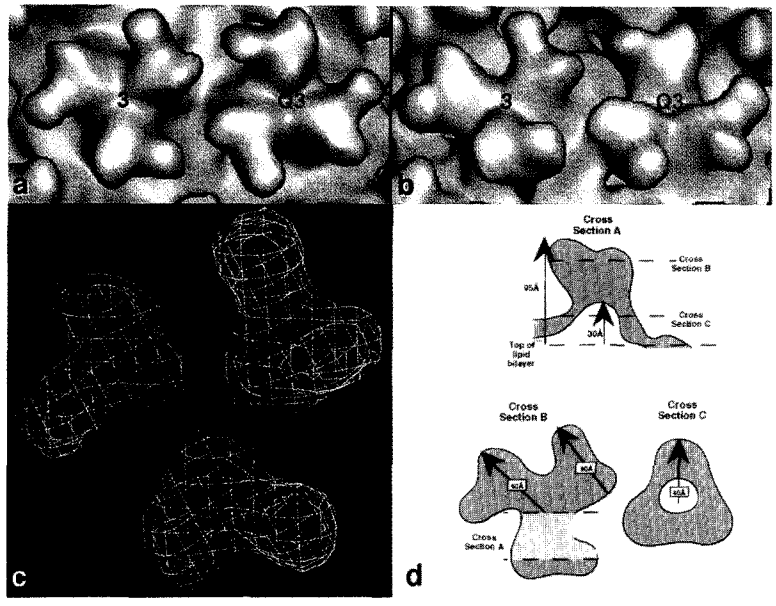

Figure 4. Glycoprotein Spike

(a) Close-up view of an adjacent pair of spikes at the icosahedral threefold (3) and quasi-threefold axes (Q3), showing nearly identical morphologies.

(b) Close-up view at a glancing angle of the two spikes shown in (a). Notice the small holes at the base of the spike.

(c) The molecular envelopes of the threefold (blue) and the quasi-threefold (red) spikes are nearly superimposable.

(d) Schematic diagrams of the RR spike structure. The side view (A) is a cross-section through an individual spike (virus center towards the bottom), showing the inner cavity that lies directly below the bulk of the spike head and extending ~30 Å above the surface of the lipid bilayer. Cross-section B is a slice through the high radius portion of the spike, viewed from outside the viral surface. Cross-section C shows the stem portion of the spike, ~25 Å above the top of the lipid bilayer.

bound with neutralizing antibody to E2 localize an epitope to the larger of the two lobes in the head group at the most distal portion of the spike (unpublished data).

Spikes on the icosahedral threefold axes contact monomers in three adjacent nucleocapsid hexamers, whereas spikes on the quasi-threefold axes contact two hexamers and one pentamer. However, at the current resolution, there is little difference in the structures of the two types of spikes (Figures 4a, 4b, and 4c). Nevertheless, the different environments at the base portion of the spikes and the potential different accessabilities of solvent and solute molecules to the interior regions of these portions of the spikes are consistent with the observations that the two spikes exhibit different sensitivity to detergent extraction (Helenius and Kartenbeck, 1980; Vénien-Bryan and Fuller, 1994). This differential extraction may be due to the greater accessibility of detergent to spikes on the threefold axes via the large holes at the three adjacent icosahedral twofold axes. In contrast, the spikes situated on the quasi-threefold axes are surrounded only by two large holes on the icosahedral twofold axes and one much smaller hole on the icosahedral fivefold axes.

Secondary structure predictions (Rost, 1993), based on the amino acid sequences of E1 and E2, suggest that both are devoid of α-helices, except in the hydrophobic regions near the C-termini. Presumably, the α-helices penetrate the lipid bilayer. The absence of helical structure in the alphavirus spikes contrasts with the largely α-helical stems of the glycoprotein spikes found in influenza virus (Bullough et al., 1994).

The Nucleocapsid Shell

The component of the nucleocapsid structure between 210 Å and 170 Å radius is organized as pentamers about the icosahedral fivefold axes and is organized as hexamers about the icosahedral twofold axes (Figures 5a and 5b). This corresponds to 240 subunits that associate in a classic quasiequivalent fashion (Caspar and Klug, 1962). At radii greater than 170 Å, the monomer subunits form contacts only within the clearly defined capsomeres (pentamers and hexamers). These capsomeres "rest" on a continuous core of density below 170 Å radius, consisting of both protein and RNA, as suggested by neutron scattering results (Jacrot, 1987). Putative protein–RNA interactions are responsible for maintaining the core structure when virions are disassembled. Viral RNA inside the core is sensitive to ribonucleases, thus suggesting it lies at the core surface exposed at sites between the pentamers and hexamers or at the center of these units (Kääriäinen and Söderlund, 1971). The density inside the ~170 Å radius must consist of the genomic RNA and the basic residues at the N-terminus of the capsid protein. Association of single-strand RNA with disordered, basic N-terminal domains of capsid proteins is prevalent in plant viruses (Harrison, 1984; Rossmann and Johnson, 1989).

The concept of quasisymmetry dictates similar monomer–monomer contacts in the formation of pentameric and hexameric capsomeres (Caspar and Klug, 1962) and, as a consequence, a quasi-twofold axis relates pentamer and hexamer subunits (A_1 and C_1 in Figure 5b). However, attempts to fit the crystallographic SCP dimer structure (Choi et al., 1991) into the 3D map of the core at the observed T = 4 quasi-twofold axes (dimers A_1C_1 and B_1D_2 in Figure 5b) showed that the dimer is not present in the core. The dimer is too short in length and cannot fill the distance representing the B_1 and D_2 subunits (Figure 5c). Furthermore, a model based on the packing of core dimers would require considerable density in the region between capsomeres, but such density is clearly absent in the reconstruction (Figure 5c). The absence of the crystallographic dimer in the virion is consistent with site-directed mutagenesis of the residues involved in stabilizing the dimer. Amino acid substitution of these residues resulted in production of mostly wild-type viruses and suggested

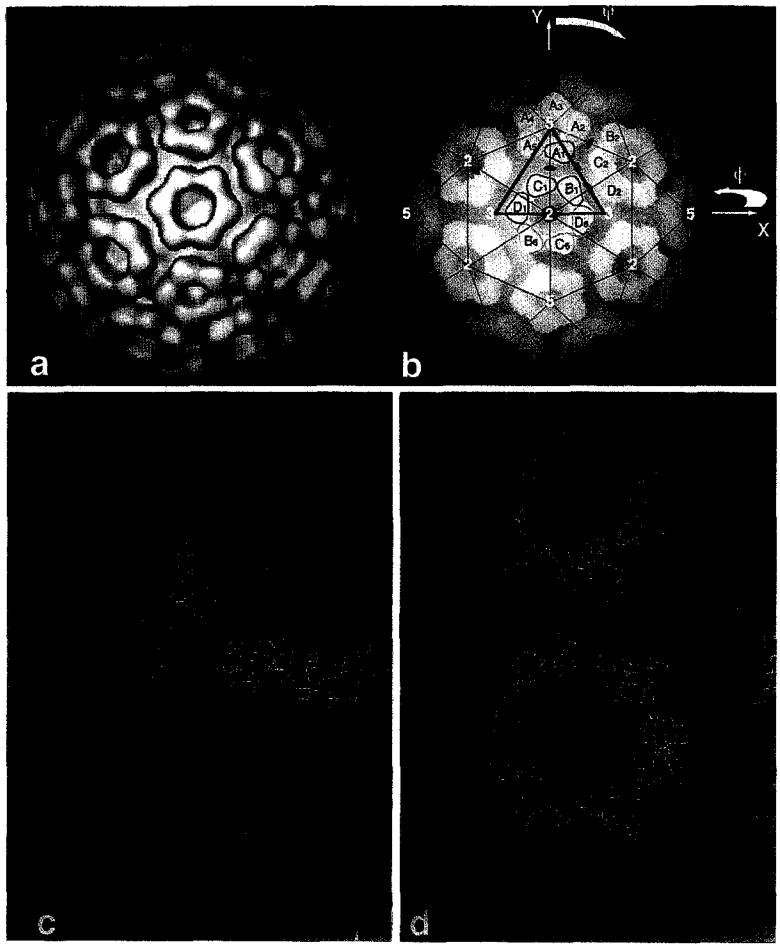

Figure 5. Structure of the RR Nucleocapsid Core

(a) Surface-shaded, twofold view of the virion reconstruction after all densities outside a radius of 210 Å were removed. The pentamer and hexamer arrangements of the nucleocapsid subunits are visible.

(b) Depth-cued representation of the map in (a) with superimposed T = 4 lattice. One icosahedral asymmetric unit lies within the triangle (red) bounded by two threefold axes and one fivefold axis. It includes four monomers (A_1, B_1, C_1, and D_1). Yellow numbers identify the icosahedral axes, and green symbols label the pseudoaxes. The polar angles are defined (as in Rossmann and Blow, 1962).

(c) Placement of the crystallographic SCP dimer Cα structure (yellow) into the observed electron density (blue). Neither the A_1C_1 nor the B_1D_2 dimers fit into the observed density.

(d) In contrast with (c), the SCP monomer (yellow) fits into the RR nucleocapsid density (blue) quite well. In agreement with cross-linking results, Lys-250 residues (denoted by asterisks) on adjacent capsomeres are ~12 Å apart.

that the dimer may not be biologically relevant (K. E. Owen and R. J. K., unpublished data).

Instead of using the crystallographically observed dimer structure to fit into the RR virus density, the structure of a single C-terminal domain of the SCP monomer was fit into the nucleocapsid portion of the reconstructed density. The latter was isolated from the whole RR virion density by zeroing all density outside a radius of 210 Å. A 6D search (three angles and three positions) produced a unique fit of all the atoms of the ordered region of the SCP atomic structure (residues 114–264) to the high density features of the EM reconstruction (Figure 5d). Sequence identity between RR and SF in their C-terminal domains is 93%, whereas RR and SIN are 68% identical (Dalgarno et al., 1983). The atomic structures of the SIN (Choi et al., 1991) and SF (H.-K. C., G. Wengler, and M. G. R., unpublished data) nucleocapsid proteins are similar, with a root mean square (rms) deviation of 0.7 Å in the Cα atoms. Hence, at the limited resolution of the EM reconstruction, the core protein structures of RR and SIN are likely to be indistinguishable.

The core proteins within pentamers and hexamers interdigitate each other with little steric interference between residues in neighboring monomers, and they form a much more extensive intersubunit interface compared with that observed in the crystallographic dimer. The monomer–monomer interface in the fitted structure involves contacts between residues 179–~191 and 219–227 on one subunit and residues 120–~126 and 212 on the other.

This core model concurs with biochemical data that identify the spatial orientation of specific residues within the intact core. Iodination of isolated cores showed that only 1 of the 4 possible tyrosine residues (Tyr-180) was accessible and, therefore, was presumed to be on the outside of the core particle (Coombs and Brown, 1987b), in agreement with the model. In addition, cross-linking studies by K. Coombs and D. T. Brown (unpublished data) suggest that lysine residues (Lys-250) on adjacent monomers are ~12 Å apart. Indeed, in agreement with the cross-linking data, the core model places Lys-250 on subunit B_1 of the hexamer ~12 Å from Lys-250 on monomer A_1 of the pentamer (Figure 5d; asterisks mark the lysine residues). The N-terminus of the ordered domain of the SCP (residue 114) lies exposed on the inner wall of the capsomere at a radius of 192 Å and points outwards. Presumably, the polypeptide reverses its direction near this point because the basic, N-terminal domain is associated with the RNA.

Membrane Structure and Glycoprotein–Nucleocapsid Interactions

The bilayer membrane is seen in cross-section (see Figure

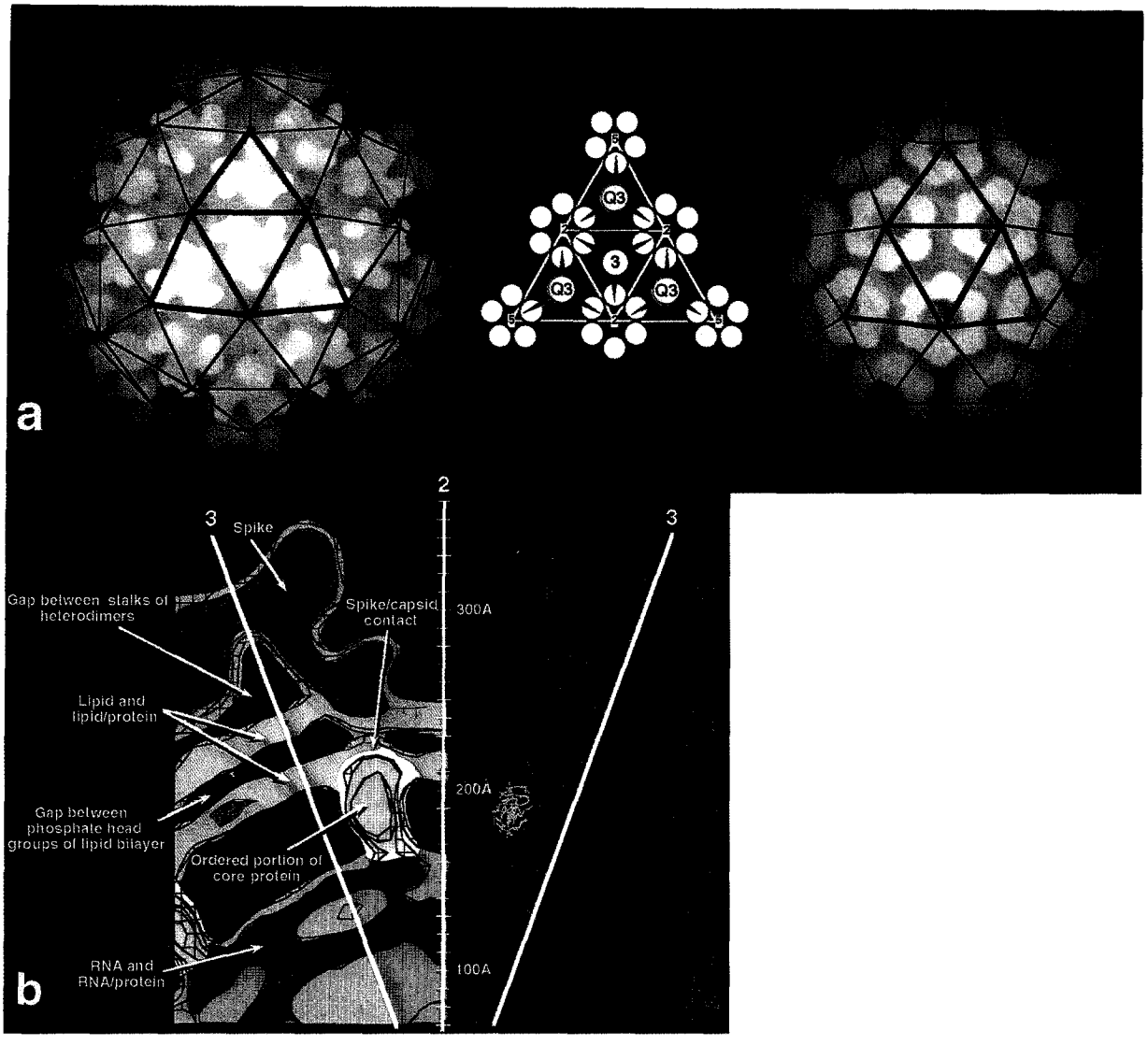

Figure 6. Mutilayer Organization of Alphaviruses

(a) Left, depth-cued representation of the 3D structure of RR (threefold view), showing the disposition of the spikes relative to the surface lattice (blue lines). Middle, schematic representation of the envelope glycoproteins as they emerge from the base of the spike, traverse the lipid bilayer membrane, and contact the underlying nucleocapsid monomers. Spikes at the icosahedral threefold (3) or quasi-threefold (Q3) are depicted by circles from which dark blue and light blue lines splay outwards at the outer surface of the membrane and then traverse the membrane and contact the underlying nucleocapsid monomers (yellow). Right, depth-cued representation of the 3D structure of the RR nucleocapsid (threefold view) showing the disposition of the core capsomeres relative to the icosahedral lattice (red lines).

(b) A 5 Å thick, detailed view of an equatorial slice of the RR image reconstruction that contains one vertical twofold axis and two adjacent threefold axes (yellow lines). Distances from the virus center are marked along the twofold axis. The density is contoured at three levels: blue (low), purple (medium), and red (high). The left half of the diagram is colored to represent different viral components: spikes (blue), phospholipid bilayer (green), core protein (yellow), and the RNA–protein interior (red). The electron density at the highest contour level (red) identifies the most icosahedrally ordered portion of the density (i.e., protein in the spikes and in the nucleocapsid capsomeres). The fit of the Cα backbone of the SCP model (yellow-green) within the density is shown at the right of the diagram.

3a) as a distinct pair of concentric, electron-dense features (phosphate head groups), with a center-to-center separation of ~32 Å and a total thickness of ~45 Å (radius from 255–210 Å), which sandwiches a lower density region (lipid hydrocarbon chains). These features are in complete agreement with small-angle X-ray solution scattering results (Harrison et al., 1971, 1974). The membrane adopts a roughly spherical shape, except where it bulges inward by 5–10 Å in the regions centered above the nucleocapsid capsomeres (see Figure 3a). At this point, the bilayer maintains its 32 Å head group separation.

Nucleocapsid–glycoprotein associations are involved during virus assembly prior to budding and also during the uncoating events that follow virus attachment and penetration. The E1 and E2 glycoproteins both contain transmembrane domains. E2 has a 31-residue cytoplasmic domain that interacts with the nucleocapsid (Garoff and Simons, 1974; Lopez et al., 1994), whereas E1 contains

only two residues (Arg-437 and Arg-438) on the inner surface of the membrane, which are dispensible for assembly and replication in SF (Barth et al., 1992). Therefore, E1 probably plays little if any role in forming the associations between spikes and the nucleocapsid core.

The RR reconstruction permits the unambiguous assignment of specific spike proteins to specific nucleocapsid protein monomers (see Figures 3a and 3b; Figure 6a). Each pentamer of the nucleocapsid is associated with five E1–E2 heterodimers that originate in five separate spikes, each of which is located on a quasi-threefold axis. Each nucleocapsid hexamer is associated with six spikes, four on quasi-threefold axes and two on icosahedral threefold axes (Figure 6a). Thus, the E1–E2 heterodimers in the 20 threefold spikes only associate with hexamer core proteins, whereas one of the E1–E2 heterodimers in each of the 60 quasi-threefold spikes associates with a pentamer protein (Figure 6a).

A close-up, cross-section view of the RR reconstruction, contoured at three different density levels, illustrates the overall organization within the multilayered RR structure and shows the putative association between the E1–E2 heterodimer and the core protein (Figure 6b). Each E1–E2 heterodimer (blue) traverses the membrane immediately above the center of each capsid monomer (yellow), where the membrane appears to be pinched and adopts a smaller thickness, presumably owing to the presence of protein on both of its sides. Here, Asn-172 in the fitted SCP model lies at the inner surface of the membrane and is juxtaposed with the glycoprotein on the external membrane surface. Thus, residues near Asn-172 may be involved in binding the 31 C-terminal, cytoplasmic residues of E2 (Helenius and Kartenbeck, 1980; Metsikkö and Garoff, 1990). Asn-172 is one of the residues believed to be involved in E2 binding on the basis of sequence comparisons between western equine encephalitis virus, eastern equine encephalitis virus, and SIN (Hahn et al., 1988). The interaction of the cytoplasmic domain of E2 with the nucleocapsid appears to be altered by site-specific mutation of Tyr-180 and Glu-183 in the nucleocapsid of SIN (Lee and Brown, 1994). This is consistent with Tyr-180 being accessible on the nucleocapsid surface and with its being near the apparent site of penetration of the membrane by the glycoprotein spike. The charge distribution on the surface of the pentameric and hexameric capsomeres is noteworthy. The outer rim of the capsomere close to the membrane is positively charged, which may complement the negatively charged head groups of the bilayer. The surface closest to the RNA is negatively charged and suggests the interface between capsomere and RNA maybe occupied by the basic, N-terminal domain of the nucleocapsid protein.

The capsid core associates with the glycoprotein spikes at the plasma membrane after the spikes have independently assembled in the endoplasmic reticulum and Golgi and after cores have assembled in the cytoplasm (Strauss and Strauss, 1994). The T = 4 arrangement of the nucleocapsid proteins might direct 80 E1–E2 trimers to assemble as a T = 4 lattice as a consequence of the one-to-one association between capsid monomers and glycoprotein heterodimers. In agreement with previous observations that virions are devoid of host cell proteins (Strauss, 1978), the presence of 80 spikes leaves little room for any additional proteins.

Conclusions

The combination of cryo-EM and X-ray crystallography to obtain high resolution information on the organization of enveloped viruses has been a fruitful approach, just as it has been in the analysis of other macromolecular complexes (Holmes, 1994). RR and related alphaviruses, such as SF and SIN, are the simplest viruses known to possess a lipid bilayer membrane. Image reconstruction of RR, together with modeling studies based on crystallographic data of the nucleocapsid protein structure of SIN, has led to the identification of specific segments of the nucleocapsid protein polypeptide that may contain the amino acids responsible for subunit contacts between monomers within the core structure and between the core and transmembrane glycoprotein.

The RR reconstruction has provided the most detailed view to date of the organization of an alphavirus and extends the previous studies of SF (Vogel et al., 1986; Vénien-Bryan and Fuller, 1994) and SIN (Fuller, 1987; Paredes et al., 1993a). Any discrepancies that may exist with previous results are largely a consequence of differences in resolution in the different studies. The reported structures for the other alphaviruses can be obtained by merely reducing the resolution of the RR reconstruction (data not shown).

The results presented here show that protein accounts for most of the surface area, with the exception of holes at the twofold and fivefold axes and also at the base of each E1–E2 heterodimer. The glycoprotein spikes exist as flower-like structures that project outward from the virus surface. The spikes have a hollow base. The component heterodimers separate immediately above the lipid bilayer and form one-to-one contacts between glycoprotein E2 and a nucleocapsid monomer on the inner surface of the membrane (Figure 6a). Contact between the outer spikes and inner core is manifested by the association of the cytoplasmic domain of E2 and the ordered, C-terminal domain of the core protein (Figure 6b). This C-terminal domain of the nucleocapsid protrudes from the surface of the core and associates with similar domains to form the distinct pentameric and hexameric capsomeres. The core structure, at a radius below 170 Å, is composed of both the genomic RNA and the basic, N-terminal domain of the nucleocapsid protein. Although the RNA is accessible to nucleases, the detailed distribution of RNA and protein remains unknown.

The role of the cavity at the base of each spike is intriguing. Does it facilitate the fusion of the viral membrane with the host membrane? A homotrimer of E1 is believed to play a role in the fusion process, and it has been suggested that rearrangement of the spike is necessary for the formation of homotrimers (Wahlberg et al., 1992).

The unique placement of the C-terminal domain of the SCP into the RR reconstruction identifies specific residues that may be involved in contacts between nucleocapsid monomers within pentamers and hexamers and between

nucleocapsid monomers and the E2 cytoplasmic domain. The interactions that maintain the arrangement of hexamers and pentamers presumably are dictated by residues in the N-terminus of the nucleocapsid (residues 1–113 using SIN numbering). The results of the present study will help guide further molecular genetic studies and measurement of other physical properties to learn about key residues that are involved in the assembly and uncoating of the virus.

Experimental Procedures

Virus Preparation

The T48 strain of RR, rescued from the full-length cDNA clone pRR64, was used as the source of virus (Kuhn et al., 1991). Mosquito cell line C6/36 (A. albopictus) was used for virus propagation. Cells were grown at 30°C in roller bottles using Eagle minimal essential medium supplemented with 10% fetal calf serum, and they were infected with virus at a multiplicity of one. Following a 36 hr incubation, cell supernatant was harvested, and virus was concentrated by precipitation in 10% PEG and 0.5 M NaCl. The virus was then resuspended and purified by sucrose density centrifugation.

Cryo-EM

The cryo-EM and image analysis procedures that were used to obtain the 3D reconstructions of RR were essentially similar to those previously reported (Baker et al., 1988; Cheng et al., 1994). The sample was maintained at near liquid nitrogen temperature with a Gatan 626 cryotransfer stage in a Philips EM420 transmission electron microscope. Micrographs were recorded under minimal dose conditions ($\sim 20\ e^{-}/Å^2$), at an objective lens defocus of under 1 μm and at 80 kV, with an instrument magnification setting of 36,000×. Enantiomorphic information (handedness) is lost in the 2D images of the particles. To determine the correct hand, image pairs were recorded in the microscope of the same field. For the second image of a pair, the goniometer stage was tilted 5° relative to the first. Two enantiomorphic reconstructions were then computed from the untilted data, and projections of each were calculated based on the orientation parameters of each particle image. Each particle image of the tilted data was then cross-correlated with the corresponding projections of the two reconstructions of the untilted data. The reconstruction of the correct hand had an average correlation coefficient of 0.41 ± 0.07, compared with 0.26 ± 0.06 for the reconstruction with the incorrect hand. Micrographs were digitized at 25 μm intervals corresponding to spacing of 7.29 Å in the specimen. Bacteriophage ΦX174 was mixed with the RR sample and was used as an internal magnification calibration standard (Olson and Baker, 1989; Cheng et al., 1994). Particle image selection was performed as previously described (Baker et al., 1991; Cheng et al., 1992).

Image Analysis

Particle images (Figure 1) were screened using a model-based approach that helped determine the relative orientations and provided quantitative criteria to select the best set of self-consistent image data (Cheng et al., 1994). Initial estimates of the phase origins (particle centers) were made by means of a cross-correlation method, with a circular-averaged image from all the digitized particle projections serving as the reference (Olson and Baker, 1989). A preliminary, 35 Å resolution, 3D reconstruction was obtained from eight particle images, at a resolution of 35 Å, with common-lines and Fourier-Bessel procedures (Crowther, 1971; Fuller, 1987; Baker et al., 1988). The resulting model was used to refine further the orientation and origin parameters of the particle images. Projected images of the 3D model, representing all unique views of the structure in 1° angular increments, were used as a reference data base for determining the orientation of newly selected particles (T. S. B. and R. H. C., unpublished data). The orientation search procedure was optimized by correlating data that had been filtered in both real space (only data between radii of 110–350 Å were used) and reciprocal space (band pass between 1/25 Å and 1/90 Å). The orientation and origin of each image was refined by maximizing the correlation coefficient between that image and the corresponding projected view of an interim reconstruction. The quality of the reconstructions significantly improved when corrections were made to adjust for slight magnification variations in the individual images (Aldroubi et al., 1992). These methods, along with cross-common lines procedures, were used to select a data set of 68 particle images to compute the final 3D reconstruction. Complete icosahedral symmetry was imposed on the final density map (Fuller, 1987). The effective resolution was estimated to be ~25 Å, based on comparing independent reconstructions (Baker et al., 1991; Cheng et al., 1992).

Model Fitting

The known atomic structure of the C-terminal domain of the SCP, being homologous to RR core protein, was oriented and positioned into each of the four independent monomeric sites of the image reconstruction that was truncated at a radius of 210 Å. Two sequential procedures were used to determine the best fit of the monomer into the EM density. An initial, coarse 3D orientational search was followed by a systematic "climb" to obtain the best fit using six refinable parameters (three orientational and three positional). The quality of fit was defined either as the average electron density or as the rms electron density taken over all the predicted atomic sites in the independent monomers. The density at each atom position was determined by an 8-point interpolation in the RR map. The number of steric clashes between neighboring monomers was assessed in terms of the number of grid points closest to each atom of one monomer that were also closest to atoms in a neighboring monomer. No attempt was made to avoid such clashes, but steric hindrance was checked graphically and found to be small for the better fits.

As a start, the center of the gravity of the SCP monomer was placed onto a designated approximate center of one of the electron density lumps (A_1 in Figure 5b) representing the RR core structure. Symmetry-related monomers within a pentamer were generated to give A_2, A_3, A_4, and A_5 by means of the nearest fivefold icosahedral axis. The monomer at A_1 was rotated into the equivalent monomer position C_1 by means of the nearest quasi-twofold axis assumed to be radial. Monomer C_1 was then reproduced to give C_1, D_1, B_6, C_6, D_6, and B_1 by virtue of the appropriate quasi-sixfold axis (Figure 5b; this sixfold axis is coincident with an icosahedral twofold axis). The position of the quasi-twofold axis is not known precisely and was, therefore, systematically adjusted to obtain the best fit. In principal, it should be necessary to refine separately the orientational and positional parameters of the four quasiequivalent monomers A_1, B_1, C_1, and D_1. However, to keep the number of refinable parameters to a minimum and, hence, to increase the significance of the resultant fit, the quasi-sixfold axis was treated as an exact sixfold axis. This gave six refinable parameters for the monomer at A_1 (three positional and three orientational), alternated with the refinement of two parameters defining the quasi-twofold axis orientation, as well as the hand of the map relative to the known absolute hand of the monomer structure.

The search procedure started by rotating the atoms of the C-terminal domain of the SCP monomer from their standard orientation by the Eulerian angles (θ1, θ2, θ3). The center of gravity of the rotated monomer was placed onto the approximate center at A_1 in the electron density from which the complete pentameric and hexameric units were then generated. The search for the best fit was pursued over all Eulerian angles ($0 \leq \theta_1 < 2\pi$; $0 \leq \theta_2 < \pi$; $0 \leq \theta_3 < 2\pi$) in increments of 30° or 20°, retaining the top 100 fits.

Each of the top fits was then subjected to exploration by "climbing" to the nearest best fit, while varying the six refinable parameters in turn. Eventually, the best fit was accepted when the angular increments had decreased from an initial 10° to a final 0.25° and when the positional increments had decreased from an initial 5 Å to a final 0.5 Å. Many of the final, best fits were the same. That is, although the climb started at a different point, the best orientation and position was found to be the same, independent of the starting parameters. The original top 100 fits, obtained by the complete Eulerian angle search, reduced itself down to about 10 distinct best fits. Two other criteria of quality of fit were, therefore, developed to differentiate them. A count was kept of atoms that were in steric collision between monomers (nclash) and of the number of atoms placed into negative density (−den). Although neither measurement was able to select clearly among the remaining best fits, a product of (nclash) × (−den) appeared to be the most sensitive quantity.

Complete explorations were performed for positions of the quasi-twofold axis using roughly 1° intervals for either hand (± 1) of the EM map. The best position of the quasi-twofold axis gave a clear preference for a unique solution, consistent with the experimentally determined hand of the EM reconstruction (Figure 5d).

Acknowledgments

The corresponding authors for this work are M. G. R. and T. S. B. We thank D. Belnap and W. Grochulski for help in determining the correct hand of the structure and S. Fuller for helpful discussions. This work was supported by National Science Foundation grants MCB-9206305 (T. S. B.) and MCB-9102855 (M. G. R) and National Institutes of Health (NIH) grants AI33982 (R. J. K.), AI11217 (M. G. R.), and GM33050 (T. S. B.). T. S. B., R. J. K., T. J. S., and M. G. R. have also benefited from an NIH program project (grant AI35212) and from a Markey Grant for the development of structural studies at Purdue University.

Received October 4, 1994; revised December 6, 1994.

References

Aldroubi, A., Trus, B. L., Unser, M., Booy, F. P., and Steven, A. C. (1992). Magnification mismatches between micrographs: corrective procedures and implications for structural analysis. Ultramicroscopy *46*, 175–188.

Aliperti, G., and Schlesinger, M. J. (1978). Evidence for an autoprotease activity of Sindbis virus capsid protein. Virology *90*, 366–369.

Anthony, R. P., and Brown, D. T. (1991). Protein–protein interactions in an alphavirus membrane. J. Virol. *65*, 1187–1194.

Baker, T. S., Drak, J., and Bina, M. (1988). Reconstruction of the three-dimensional structure of simian virus 40 and visualization of the chromatin core. Proc. Natl. Acad. Sci. USA *85*, 422–426.

Baker, T. S., Newcomb, W. W., Olson, N. H., Cowsert, L. M., Olson, C., and Brow, J. C. (1991). Structures of bovine and human papillomaviruses. Analysis by cryoelectron microscopy and three-dimensional reconstruction. Biophys. J. *60*, 1445–1456.

Barth, B. U., Suomalainen, M., Liljeström, P., and Garoff, H. (1992). Alphavirus assembly and entry: role of the cytoplasmic tail of the E1 spike subunit. J. Virol. *66*, 7560–7564.

Bullough, P. A., Hughson, F. M., Skehel, J. J., and Wiley, D. C. (1994). Structure of the influenza haemagglutinin at the pH of membrane fusion. Nature *371*, 37–43.

Caspar, D. L. D., and Klug, A. (1962). Physical principles in the construction of regular viruses. Cold Spring Harbor Symp. Quant. Biol. *27*, 1–24.

Cheng, R. H., Olson, N. H., and Baker, T. S. (1992). Cauliflower mosaic virus: a 420 subunit (T = 7) multilayer structure. Virology *186*, 655–668.

Cheng, R. H., Reddy, V. S., Olson, N. H., Fisher, A. J., Baker, T. S., and Johnson, J. E. (1994). Functional implications of quasi-equivalence in a T = 3 icosahedral animal virus established by cryo-electron microscopy and X-ray crystallography. Structure *2*, 271–282.

Choi, H.-K., Tong, L., Minor, W., Dumas, P., Boege, U., Rossmann, M. G., and Wengler, G. (1991). Structure of Sindbis virus core protein reveals a chymotrypsin-like serine proteinase and the organization of the virion. Nature *354*, 37–43.

Coombs, K., and Brown, D. T. (1987a). Organization of the Sindbis virus nucleocapsid as revealed by bifunctional cross-linking agents. J. Mol. Biol. *195*, 359–371.

Coombs, K., and Brown, D. T. (1987b). Topological organization of Sindbis virus capsid protein in isolated nucleocapsids. Virus Res. *7*, 131–149.

Crowther, R. A. (1971). Procedures for three-dimensional reconstruction of spherical viruses by Fourier synthesis from electron micrographs. Phil. Trans. Roy. Soc. (Lond.) B *261*, 221–230.

Dalgarno, L., Rice, C. M., and Strauss, J. H. (1983). Ross River virus 26S RNA: complete nucleotide sequence and deduced sequence of the encoded structural proteins. Virology *129*, 170–187.

Dalrymple, J. M., Schlesinger, S., and Russell, P. K. (1976). Antigenic characterization of two Sindbis envelope glycoproteins separated by isoelectric focussing. Virology *69*, 93–103.

Doherty, R. L., Whitehead, R. H., Gorman, B. M., and O'Gower, A. K. (1963). The isolation of a third group A arbovirus in Australia, with preliminary observations on its relationship to epidemic polyarthritis. Aust. J. Sci. *26*, 183–184.

Faragher, S. G., Meek, A. D. J., Rice, C. M., and Dalgarno, L. (1988). Genome sequences of a mouse-avirulent and a mouse-virulent strain of Ross River virus. Virology *163*, 509–526.

Fuller, S. D. (1987). The T = 4 envelope of Sindbis virus is organized by interactions with a complementary T = 3 capsid. Cell *48*, 923–934.

Garoff, H., and Simons, K. (1974). Location of the spike glycoproteins in the Semliki Forest virus membrane. Proc. Natl. Acad. Sci. USA *71*, 3988–3992.

Garoff, H., Simons, K., and Renkonen, O. (1974). Isolation and characterization of the membrane proteins of Semliki Forest virus. Virology *61*, 493–504.

Garoff, H., Frischauf, A. M., Simons, K., Lehrach, H., and Delius, H. (1980). Nucleotide sequence of cDNA coding for Semliki Forest virus membrane glycoproteins. Nature *288*, 236–241.

Geigenmüller-Gnirke, U., Nitschko, H., and Schlesinger, S. (1993). Deletion analysis of the capsid protein of Sindbis virus: identification of the RNA binding region. J. Virol. *7*, 1620–1626.

Hahn, C. S., Lustig, S., Strauss, E. G., and Strauss, J. H. (1988). Western equine encephalitis virus is a recombinant virus. Proc. Natl. Acad Sci. USA *85*, 5997–6001.

Harrison, S. C. (1984). Multiple modes of subunit association in the structures of simple spherical viruses. Trends Biochem. Sci. *9*, 345–351.

Harrison, S. C., David, A., Jumblatt, J., and Darnell, J. E. (1971). Lipid and protein organization in Sindbis virus. J. Mol. Biol. *60*, 523–528.

Harrison, S. C., Jack, A., Goodenough, D., and Sefton, B. M. (1974). Structural studies of spherical viruses. J. Supramol. Struct. *2*, 486–495.

Harrison, S. C., Strong, R. K., Schlesinger, S., and Schlesinger, M. J. (1992). Crystallization of Sindbis virus and its nucleocapsid. J. Mol. Biol. *226*, 277–280.

Helenius, A., and Kartenbeck, J. (1980). The effects of octylglucoside on the Semliki Forest virus membrane: evidence for a spike–protein–nucleocapsid interaction. Eur. J. Biochem. *106*, 613–618.

Holmes, K. C. (1994). Solving the structure of macromolecular complexes. Structure *2*, 589–593.

Horzinek, M. C., and Mussgay, M. (1969). Studies on the nucleocapsid structure of group A arboviruses. J. Virol. *4*, 514–520.

Jacrot, B. (1987). Neutron scattering. In Animal Virus Structure, M. V. Nermut and A. C. Steven, eds. (New York: Elsevier Science), pp. 89–95.

Kääriäinen, L., and Söderlund, H. (1971). Properties of Semliki Forest virus nucleocapsid. I. Sensitivity to pancreatic ribonuclease. Virology *43*, 291–299.

Kay, B. H., and Aaskov, J. G. (1989). Ross River virus (epidemic polyarthritis). In The Arboviruses: Epidemiology and Ecology, T. P. Monath, ed. (Boca Raton, Florida: CRC Press), pp. 93–112.

Kenney, J. M., Sjöberg, M., Garoff, H., and Fuller, S. D. (1994). Visualization of fusion activation in the Semliki Forest virus spike. Structure *2*, 823–832.

Kuhn, R. J., Niesters, H. G. M., Hong, Z., and Strauss, J. H. (1991). Infectious RNA transcripts from Ross River virus cDNA clones and the construction and characterization of defined chimeras with Sindbis virus. Virology *182*, 430–441.

Lee, H., and Brown, D. T. (1994). Mutations in an exposed domain of Sindbis virus capsid protein result in the production of noninfectious virions and morphological variants. Virology *202*, 390–400.

Lopez, S., Yao, J.-S., Kuhn, R. J., Strauss, E. G., and Strauss, J. H. (1994). Nucleocapsid–glycoprotein interactions required for assembly of alphaviruses. J. Virol. *68*, 1316–1323.

Marshall, I. D., and Miles, J. A. R. (1984). Ross River virus and epi-

demic polyarthritis. In Current Topics in Vector Research, K. F. Harris, ed. (New York: Praeger Publications), pp. 31–56.

Mayne, J. T., Rice, C. R., Strauss, E. G., Hunkapiller, M. W., and Strauss, J. H. (1984). Biochemical studies of the maturation of the small Sindbis virus glycoprotein E3. Virology *134*, 338–357.

Metsikkö, K., and Garoff, H. (1990). Oligomers of the cytoplasmic domain of the p62/E2 membrane protein of Semliki Forest virus bind to the nucleocapsid *in vitro*. J. Virol. *64*, 4678–4683.

Olson, N. H., and Baker, T. S. (1989). Magnification calibration and the determination of spherical virus diameters using cryoEM. Ultramicroscopy *30*, 281–298.

Paredes, A. M., Brown, D. T., Rothnagel, R., Chiu, W., Johnston, R. E., and Prasad, B. V. V. (1993a). Three-dimensional structure of a membrane-containing virus. Proc. Natl. Acad. Sci. USA *90*, 9095–9099.

Paredes, A. M., Simon, M. L., and Brown, D. T. (1993b). The mass of the Sindbis virus nucleocapsid suggests it has T = 4 icosahedral symmetry. Virology *187*, 329–332.

Rice, C. M., and Strauss, J. H. (1981). Nucleotide sequence of the 26S mRNA of Sindbis virus and deduced sequence of the encoded virus structural proteins. Proc. Natl. Acad. Sci. USA *78*, 2062–2066.

Rice, C. M., and Strauss, J. H. (1982). Association of Sindbis virion glycoproteins and their precursors. J. Mol. Biol. *154*, 325–348.

Rossmann, M. G., and Blow, D. M. (1962). The detection of subunits within the crystallographic asymmetric unit. Acta Cryst. *15*, 24–31.

Rossmann, M. G., and Johnson, J. E. (1989). Icosahedral RNA virus structure. Annu. Rev. Biochem. *58*, 533–573.

Rost, R. (1993). Progress in protein structure prediction. Trends Biochem. Sci. *18*, 120–123.

Simmons, D. T., and Strauss, J. H. (1974). Translation of Sindbis virus 26S RNA and 49S RNA in lysates of rabbit reticulocytes. J. Mol. Biol. *86*, 397–409.

Strauss, E. G. (1978). Mutants of Sindbis virus III. Host polypeptides present in purified HR and *ts* 103 particles. J. Virol. *28*, 466–474.

Strauss, J. H., and Strauss, E. G. (1994). The alphaviruses: gene expression, replication, evolution. Microbiol. Rev. *58*, 491–562.

Stubbs, M. J., Miller, A., Sizer, P. J. H., Stephenson, J. R., and Crooks, A. J. (1991). X-ray solution scattering of Sindbis virus: changes in conformation induced at low pH. J. Mol. Biol. *221*, 39–42.

Tong, L., Choi, H. K., Minor, W., and Rossmann, M. G. (1992). The structure determination of Sindbis virus core protein using isomorphous replacement and molecular replacement averaging between two crystal forms. Acta Cryst. *48*, 430–442.

Tong, L., Wengler, G., and Rossmann, M. G. (1993). Refined structure of the Sindbis virus core protein and comparison with other chymotrypsin-like serine proteinase structures. J. Mol. Biol. *230*, 228–247.

Ubol, S., and Griffin, D. E. (1991). Identification of a putative alphavirus receptor on mouse neural cells. J. Virol. *65*, 6913–6921.

Vénien-Bryan, C., and Fuller, S. D. (1994). The organization of the spike complex of Semliki Forest virus. J. Mol. Biol. *236*, 572–583.

Vogel, R. H., Provencher, S. W., von Bonsdorff, C.-H., Adrian, M., and Dubochet, J. (1986). Envelope structure of Semliki Forest virus reconstructed from cryo-electron micrographs. Nature *320*, 533–535.

Vrati, S., Faragher, S. G., Weir, R. C., and Dalgarno, L. (1986). Ross River virus mutant with a deletion in the E2 gene: properties of the virion, virus-specific macromolecule synthesis, and attenuation of virulence for mice. Virology *151*, 222–232.

Wahlberg, J. M., Bron, R., Wilschut, J., and Garoff, H. (1992). Membrane fusion of Semliki Forest virus involves homotrimers of the fusion protein. J. Virol. *66*, 7309–7318.

Wang, K.-S., Schmaljohn, A. L., Kuhn, R. J., and Strauss, J. H. (1991). Antiidiotypic antibodies as probes for the Sindbis virus receptor. Virology *181*, 694–702.

Weiss, B., Geigenmüller-Gnirke, U., and Schlesinger, S. (1994). Interaction between Sindbis virus RNAs and a 68 amino acid derivative of the viral capsid protein further defines the capsid binding site. Nucl. Acids Res. *22*, 780–786.

Wengler, G., Wurkner, D., and Wengler, G. (1992). Identification of a sequence element in the alphavirus core protein which mediates interaction of cores with ribosomes and the disassembly of cores. Virology *191*, 880–888.

Ziemiecki, A., and Garoff, H. (1978). Subunit composition of the membrane glycoprotein complex of Semliki Forest virus. J. Mol. Biol. *122*, 259–269.

Protein Data Bank Accession Number

The accession number for the SCP monomer sequence reported in this paper is 2SNV.